The Inhibitory Activity of Plants from Central Argentina on *p*-Hydroxyphenylpyruvate Dioxygenase. Isolation and Mechanism of Inhibition of a Flavanone from *Flourensia oolepis*

DOI 10.1055/s-0035-1557864
Planta Med

Publishing House and Copyright:
© 2015 by
Georg Thieme Verlag KG
Rüdigerstraße 14
70469 Stuttgart
ISSN 0032-0943

The Inhibitory Activity of Plants from Central Argentina on *p*-Hydroxyphenylpyruvate Dioxygenase. Isolation and Mechanism of Inhibition of a Flavanone from *Flourensia oolepis*

Authors María Eugenia Chiari[1], Leonardo Tosoni[2], Mariana Belén Joray[1], Georgina Natalia Diaz Napal[1], Sara María Palacios[1], Gustavo Miguel Ruiz[3], Domingo Mariano A. Vera[2], María Cecilia Carpinella[1]

Affiliations
[1] Fine Chemical and Natural Products Laboratory, School of Chemistry, Catholic University of Córdoba, Argentina
[2] Department of Chemistry, College of Exact and Natural Sciences, National University of Mar del Plata, Argentina
[3] Herbarium Marcelino Sayago, School of Agricultural Science, Catholic University of Córdoba, Argentina

Key words
- *Flourensia oolepis*
- Asteraceae
- HPPD inhibitors
- Argentinian native plants
- pinocembrin
- molecular docking

received Dec. 9, 2014
revised April 1, 2015
accepted June 14, 2015

Bibliography
DOI http://dx.doi.org/10.1055/s-0035-1557864
Published online
Planta Med © Georg Thieme Verlag KG Stuttgart · New York · ISSN 0032-0943

Correspondence
Prof. Dr. María Cecilia Carpinella
Laboratorio de Química Fina y Productos Naturales
Facultad de Ciencias Químicas
Universidad Católica de Córdoba
Avda. Armada Argentina 3555
X5016DHK Córdoba
Argentina
Phone: + 54 35 14 93 80 00, ext. 611
Fax: + 54 35 14 93 80 61
ceciliacarpinella@ucc.edu.ar

Correspondence
Prof. Dr. Domingo Mariano A. Vera
Departamento de Química
Facultad de Ciencias Exactas y Naturales
Universidad Nacional de Mar del Plata
Funes 3350
B7602AYL Mar del Plata
Argentina
Phone: + 54 22 34 75 61 67
dmavera@yahoo.com

Abstract

The enzyme 4-hydroxyphenylpyruvate dioxygenase catalyzes the second step in the tyrosine degradation pathway. In mammals, this enzyme is the molecular target of drugs used for the treatment of metabolic disorders associated with defects in the tyrosine catabolism, mainly the fatal hereditary disease tyrosinemia type 1. This study evaluated the inhibitory effect of 91 extracts on 4-hydroxyphenylpyruvate dioxygenase from mostly native plants from central Argentina. *Flourensia oolepis* ethanol extract showed itself to be the most effective, and bioguided fractionation yielded pinocembrin (**1**) as its active principle. This flavanone, with an IC_{50} value of 73.1 µM and a K_I of 13.7 µM, behaved as a reversible inhibitor of the enzyme and as a noncompetitive inhibitor. Molecular modeling studies confirmed the inhibitory potency of **1** and explained its activity by means of *in silico* determination of its binding mode in comparison to inhibitors of known activity, cocrystallized with 4-hydroxyphenylpyruvate dioxygenase. The main structural determinants that confer its potency are discussed. Analysis of the binding mode of the flavanone **1** with 4-hydroxyphenylpyruvate dioxygenase revealed the basis of the noncompetitive reversible mechanism of inhibition at the molecular level, which seems to be a common feature in this ubiquitous family of natural compounds. The resulting information may establish the basis for obtaining novel 4-hydroxyphenylpyruvate dioxygenase inhibitors for the treatment of tyrosinemia type 1 and other disorders associated with tyrosinase catabolism.

Abbreviations

AcOEt:	ethyl acetate
Et_2O:	diethyl ether
HGA:	homogentisate
HPP:	4-hydroxyphenylpyruvate
HPPD:	4-hydroxyphenylpyruvate dioxygenase
IC_{50}:	inhibitor concentration leading to 50% activity loss
K_I:	inhibition constant
K_m:	Michaelis-Menten constant
MeOH:	methanol
NTBC:	nitisinone
QM:	quantum mechanics
TH1:	tyrosinemia type 1

Supporting information available online at http://www.thieme-connect.de/products

Introduction

HPPD (EC 1.13.11.27) is an iron-dependent, nonheme oxygenase enzyme present in most organisms. It is involved in the second step of the tyrosine degradation pathway, catalyzing the conversion of HPP to HGA [1]. The latter intermediate will be finally converted, by successive reactions involving other enzymes, into the energy contributors acetoacetate and fumarate [1]. In mammals, inborn defects in all of the enzymes involved in this pathway lead to a number of serious metabolic disorders [2], including fatal hereditary TH1 [3]. This disease is caused by a functional deficiency of the enzyme fumarylacetoacetate hydrolase that catalyzes the final step in the catabolism of tyrosine, leading to the upstream accumulation of the hepatotoxic and nephrotoxic metabolites, fumarylacetoacetate, maleylacetoacetate, and succinylacetone [3,4]. High levels of these components result in the characteristics of the disease, which, if untreated, is lethal in both its acute and chronic forms [3,4].

Table 1 Inhibitory activity of the most effective ethanol extracts of native and endemic plants from central Argentina and pinocembrin (**1**) on HPPD.

Species	Inhibition (%)*	IC_{50} (μg/mL/μM) values and 95% confidence limits (lower, upper)
Achyrocline satureioides	93.90 ± 4.12	186.686 (89.319–390.192)
Baccharis coridifolia	94.63 ± 1.26	157.857 (40.603–605.971)
Flourensia oolepis	85.87 ± 0.40	65.724 (26.523–162.864)
Ophryosporus charua	85.27 ± 8.48	126.380 (8.352–1935.510)
Salvia cuspidata	92.52 ± 7.48	120.166 (20.328–710.347)
Solanum sisymbriifolium	84.88 ± 5.14	170.915 (39.512–739.307)
1		18.714 (6.755–51.841)/73.067 (26.385–202.339)
Mesotrione	100.00	0.011 (0.0006–0.211)/0.033 (0.002–0.623)

* Data represent the mean ± standard error of the evaluated parameter in duplicate of three different repetitions. Extracts were tested at 250 μg/mL

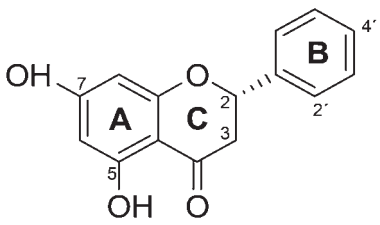

Fig. 1 Chemical structure of pinocembrin (**1**).

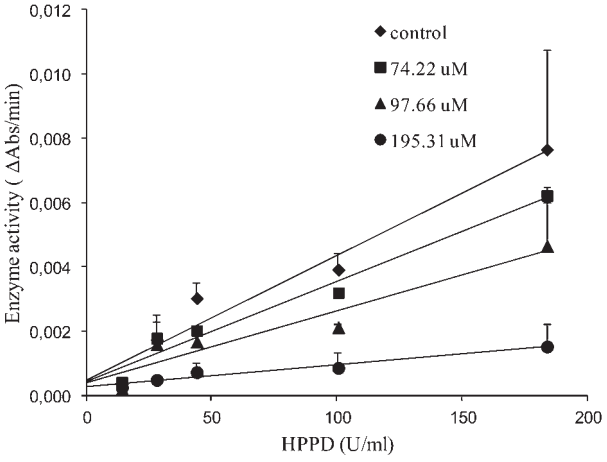

Fig. 2 Effects of concentrations of HPPD on its activity for the catalysis of the enol form of HPP at different concentrations of pinocembrin (**1**). Values are the mean ± SE of two separate experiments.

Preventing the production of these harmful metabolites by blocking HPPD activity is thus the main therapy for this life-threatening disorder [3]. Moreover, HPPD inhibition alleviates the symptoms of the other less severe metabolic diseases associated with the catabolic cascade of tyrosine [1]. Previous trials have also tested HPPD inhibitors for the treatment of Parkinson's disease [5], thus enlarging the spectrum of action of the molecules with this property.

As far as we know, very little information about plant-derived products showing HPPD inhibitory activity has been found in the literature [6–9], even when the starting point for the synthesis of NTBC, a herbicide which is also used as the therapy of choice for the treatment of TH1 [3], was the natural *β*-triketone, leptospermone [10]. The search for alternative HPPD inhibitors obtained from plants thus seems well worth investigating.

As part of our ongoing effort to find enzyme inhibitors from plants [11–13], 91 extracts from mostly native species from central Argentina were screened *in vitro* for anti-HPPD activity. The responsible active principle from the most effective plant was isolated and identified. We describe here in detail the inhibitory potency, kinetic behavior, parameters of inhibition, and interaction of this inhibitor with the enzyme.

Results

In order to obtain agents with inhibitory activity on HPPD, extracts derived from 91 plants from central Argentina were screened. In this study, the ethanol extracts from *Dysphania ambrosioides* (L.) Mosyakin & Clemants (Chenopodiaceae), *Otholobium higuerilla* (Gillies ex Hook.) J.W. Grimes (Fabaceae), and *Solanum palinacanthum* Dunal (Solanaceae) showed inhibitory effects with percentages ranging from 71 to 78% (**Table 1 S**, Supporting Information), while the extracts from *Achyrocline satureioides* (Lam.) DC. (Asteraceae), *Baccharis coridifolia* DC. (Asteraceae), *Flourensia oolepis* S.F. Blake (Asteraceae), *Ophryosporus charua* (Griseb.) Hieron. (Asteraceae), *Salvia cuspidata* Ruiz & Pav. (Lamiaceae), and *Solanum sisymbriifolium* Lam. (Solanaceae) showed at least 85% inhibition when tested at 250 μg/mL (**Table 1**). Among these, *F. oolepis* extract was the most effective, with an IC_{50} of 65.7 μg/mL, followed by *S. cuspidata* (IC_{50} = 120.2 μg/mL) and *O. charua* (IC_{50} = 126.4 μg/mL) ones (**Table 1**). Given these results, *F. oolepis* was selected to be submitted to bioguided fractionation in order to isolate its anti-HPPD principle. The flavanone identified as pinocembrin (**1**) (**Fig. 1**) [14] was obtained from this process, and showed an IC_{50} value of 73.1 μM (18.7 μg/mL) (**Table 1**).

The inhibitory mechanism of compound **1** on HPPD was then studied. The plots of the remaining enzyme activity versus the concentration of enzyme in the presence of different concentrations of **1** gave a series of straight lines, which all passed through the origin. Increasing the inhibitor concentration resulted in a decrease in the slope of the lines, thus indicating that the enzyme undergoes a reversible inhibition (**Fig. 2**).

We decided to further characterize the HPPD interaction with compound **1** by evaluating the type of inhibition on the enzyme. The kinetic of inactivation was analyzed by the Lineweaver-Burk double reciprocal method. The plots obtained yield a family of straight lines with different slopes with a common intercept in the X-axis (**Fig. 3**). With increasing concentrations of the flavanone, V_{max} decreased while K_m remained unchanged. These results showed that **1** was a noncompetitive inhibitor. The inhibi-

tion constants for inhibitor binding with the free enzyme or enzyme-substrate complex, K_I or K_{IS}, respectively, were the same in quantity (K_I = 13.7 µM). All kinetic parameters, determined by Lineweaver-Burk plots, are summarized in ◉ **Table 2**.

Prior to discussing the binding modes of **1**, the calculation protocol used for the molecular docking simulation was validated by challenging the procedure to reproduce both the position and the pose of the cocrystallized inhibitors in the X-ray structures and to correlate the docking energies against known experimental activities for the whole panel of compounds A–M (◉ **Fig. 4**). With this aim, different models were built and evaluated (for further details, see Materials and Methods section and Supporting Information), and the two with the best correlations to the experimental data were discussed further. As shown in ◉ **Fig. 5**, the structure of the complex DAS869/*R. novergicus* HPPD was closely reproduced by the procedure. The correlations between the IC_{50} s

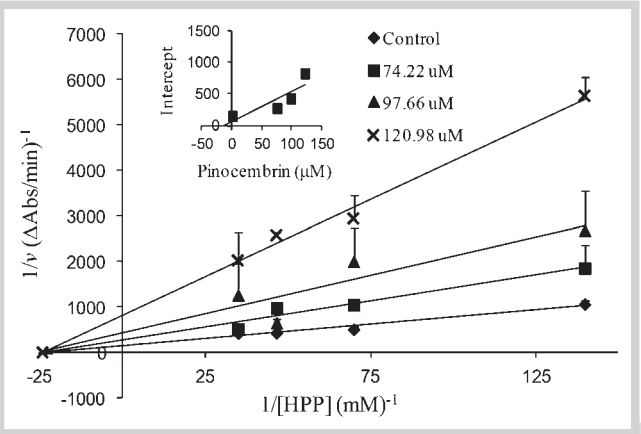

Fig. 3 Lineweaver-Burk plots for the inhibition of HPPD in the presence of different concentrations of pinocembrin (**1**). The insets represent the plot of the vertical intercepts ($1/V_{max\ app}$) versus pinocembrin concentrations to determine the inhibition constants. The lines were drawn using linear least squares fit. Values are the mean ± SE of two separate experiments.

Table 2 Kinetic parameters of the enzyme and inhibition constants with pinocembrin (**1**).

Kinetic parameters	
K_m (µM)	44.43
V_{max} (ΔAbs/min)	0.007
K_I (µM)	13.75
K_{IS} (µM)	13.75

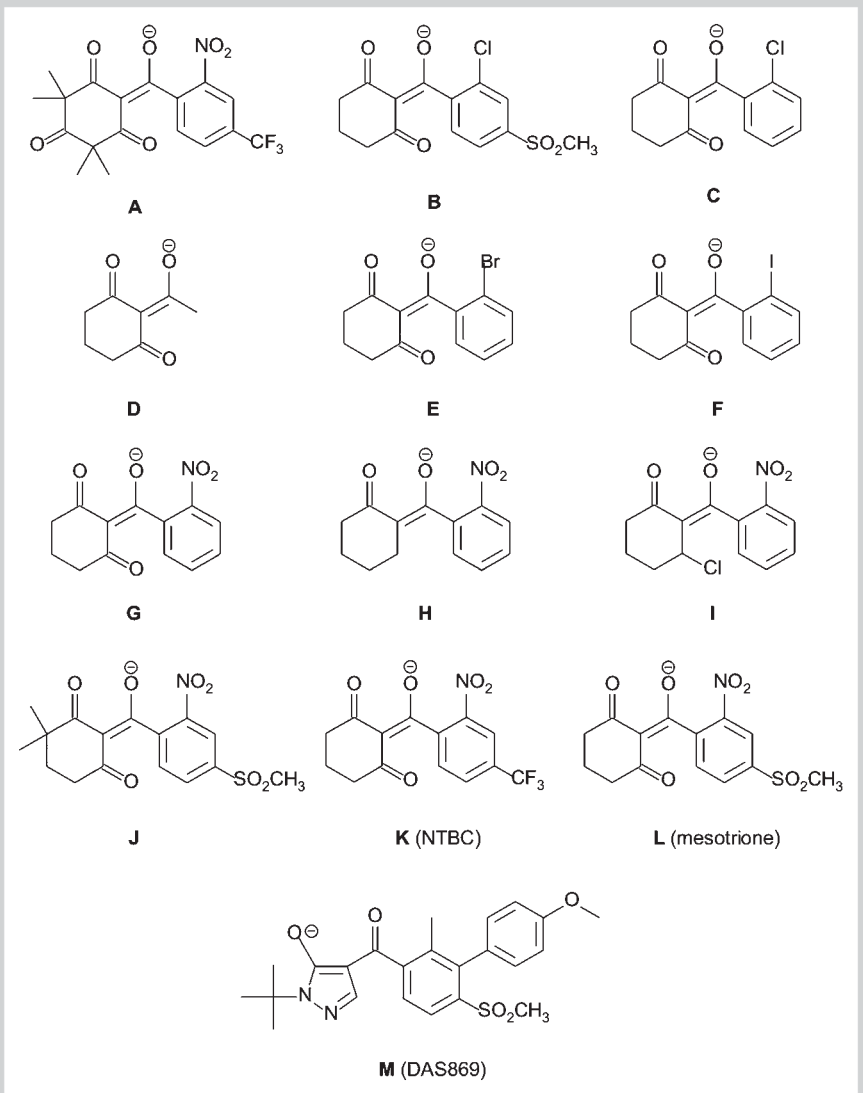

Fig. 4 Family of HPPD inhibitors of known activity and inhibitors cocrystallized with HPPD in their most likely protonation state at physiological pH.

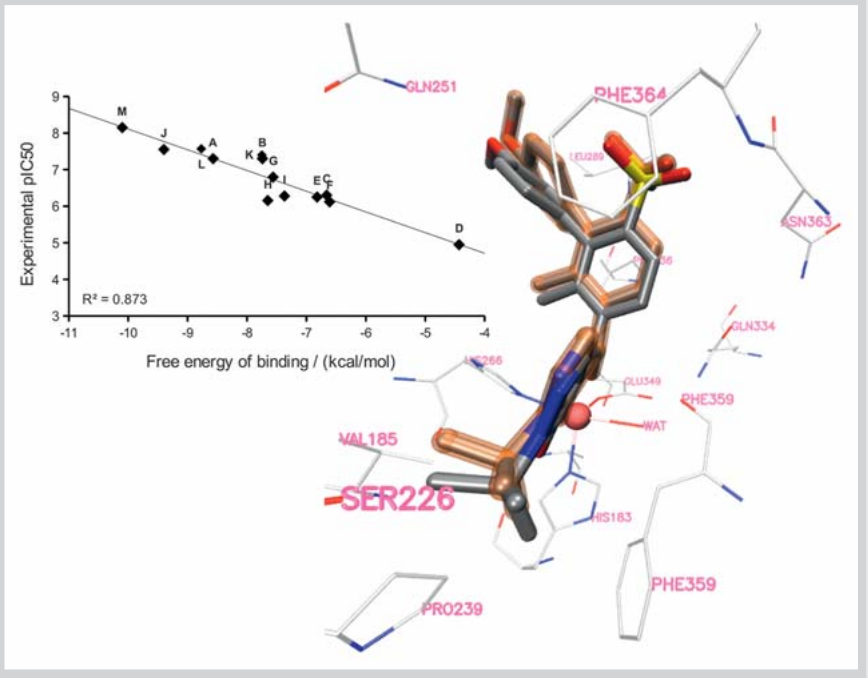

Fig. 5 **A** Correlation between the free energies of binding and the experimental IC_{50} s for the panel of known compounds A–M. The letter codes correspond to the structures on ◉ **Fig. 4**. **B** Superimposition of the experimental structure of DAS869 cocrystallized in the active site (highlighted in orange) of *R. novergicus* HPPD and the lowest energy structure of the first lowest energy cluster found by the docking procedure. Key residues are shown in thinner tubes; the iron ion is shown as a red sphere. (Color figure available online only.)

reported in the literaure [15–21] and the free energies of binding (= $RT\ln K_i$) found for the set of known inhibitors were also very good ($R^2 = 0.873$, ◉ **Fig. 5**; further details in **Table 2 S**, Supporting Information). In the absence of the water molecule as part of the receptor structure (Model III, **Fig. 4 S**, Supporting Information), the correlation with the experimental activities was still good ($R^2 = 0.867$), although the coincidence between the lowest energy docked structure and the X-ray structure was slightly poorer than that obtained by including the water molecule (the three superimposed structures are shown in **Fig. 2 S**, Supporting Information). The structure of the NTBC cocrystallized inhibitor was not as closely reproduced as in the case of DAS869 onto the mammal protein shown in ◉ **Fig. 5**; however, the correlation with the experimental IC_{50} s was good ($R^2 = 0.861$, **Table 3 S** and **Fig. 3 S**, Supporting Information). The overall good agreement with the available experimental information allowed us to attempt to describe in detail the binding of compound **1** to HPPD within this approach.

The tight binding inhibitors NTBC and DAS869 were cocrystallized with their β-dioxo systems coordinated to the metal, and the docking simulations revealed a clear preference of these inhibitors for the coordinated poses (all of the 500 lowest energy docked conformations obtained fell on the metal coordination sphere). In contrast, compound **1** was found to have a comparable affinity for a different binding mode in its phenolate form ($\mathbf{1}^-$) and it was not directly bound to the iron in its neutral form (the one most likely to occur at physiological pH due to its relatively high pKa value).

In the case of $\mathbf{1}^-$, this was still capable of mimicking the DAS869 and NTBC in its second lowest energy cluster. This similarity is clear in ◉ **Fig. 6 a**, where $\mathbf{1}^-$ and the experimental structure of NTBC are superimposed (Model II). This can also be noted by comparing the poses in ◉ **Fig. 6 c, d** to DAS869 (Model I, ◉ **Fig. 5**). The phenyl B-ring was forming a π-π stacking with the Phe364 and also interacting with the same hydrophobic and aromatic residues as the $-CF_3$ group of NTBC. The main difference relies on the free 7-OH function, absent in NTBC, which is involved in a strong interaction as both an H-bond donor and acceptor, with a conserved couple of serine and asparragine residues (Ser230 and Asn245 and the corresponding Ser226 and Asn241 in the bacterium and mammal sequences, respectively).

However, as noted above, the pose in ◉ **Fig. 6 a** is the second lowest energy structure, since the first lowest one found for $\mathbf{1}^-$ is not interacting with the metal. Indeed, the pose of lowest energy shown in ◉ **Fig. 6 b** (1.28 kcal/mol more stable than that shown in ◉ **Fig. 6 a**) is in the upper entry to the coordination site, as shown by superimposing this structure on the crystal structure of the coordinated NTBC (◉ **Fig. 6 b**). This site will be discussed just with Model II, since the experimental structure is complete enough to allow us to cover the whole binding region, including both entrances to the site (see below). It is recalled here that both mesotrione and NTBC anions have no pose in this region.

With respect to the neutral form of **1**, this was similar to its phenolate (◉ **Fig. 6 b**) and is shown in ◉ **Fig. 7 a**, where the binding domain scanned is shown together with the experimental structure of NTBC; it can be seen that NTBC and **1** poses are clearly not overlapping. As shown in ◉ **Fig. 7 b, c**, the lowest energy docked structure of the neutral **1** accommodates in the entrance of the site with its 7-OH, cromene, and carbonyl oxygens involved in four H-bonds and its B-ring comprised of hydrophobic interactions with the residues which shape the top entrance of the coordination site (◉ **Fig. 7 d, e**). Secondary binding modes of the neutral **1** were found closer to the iron, but none of them was directly interacting with Fe(II), i.e., mimicking the DAS869, NTBC or mesotrione binding modes. [The second lowest energy pose of the neutral **1** within Model II (1.46 and 1.67 kcal/mol less stable than the lowest one, respectively) as well as the two lowest energy poses found with Model I (docking region restricted to the iron coordination site) were closer to the iron. These secondary modes of neutral compound **1** are shown in **Fig. 9 S**, Supporting Information.] In addition, the poses of **1** were clearly less stable than those found for these coordinating inhibitors (binding energies by the docking are summarized in ◉ **Table 3**).

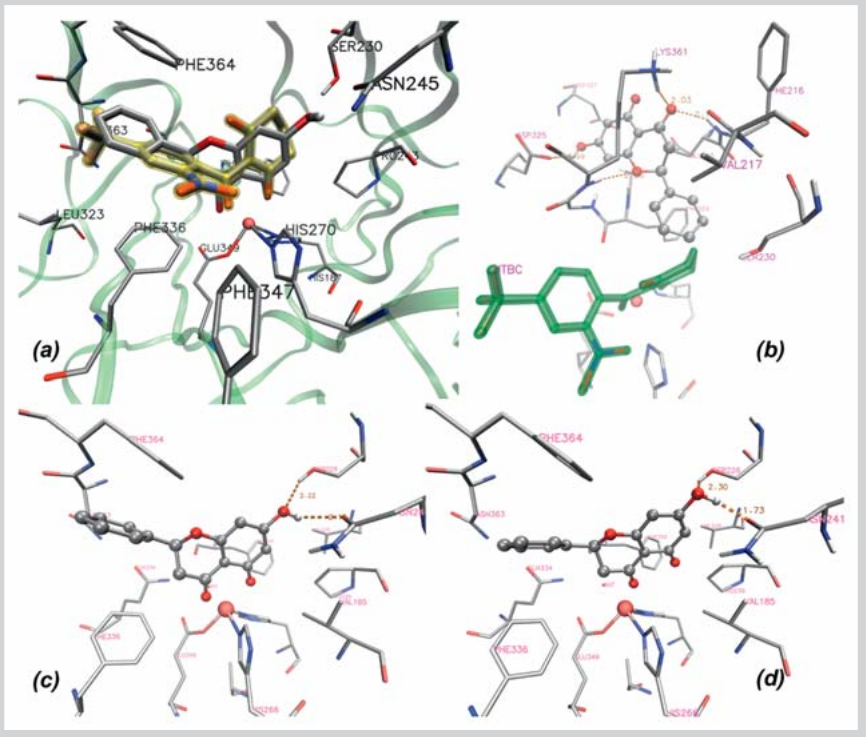

Fig. 6 Poses of compound **1** as phenolate (**1**$^-$): **a** Superimposition of the experimental structure of NTBC cocrystallized onto the *S. avermitilis* HPPD (highlighted in yellow) and the second lowest energy structure of **1**$^-$. As with NTBC, **1**$^-$ interacts as a bidentate ligand to the Fe(II) through its *β*-dioxo system. The B-ring features a *π-π* stacking with Phe364 and has hydrophobic contacts with the same residues as NTBC. **b** The lowest energy pose of **1**$^-$, however, does not overlap with NTBC (shaded in green). Also, it does not interact with the coordination site. **c, d** The two lowest energy poses of **1**$^-$ in the coordination site of *R. novergicus* HPPD are similar to the one in (**a**). Both poses have similar energies (within 0.2 kcal/mol of difference). The main difference found was that the interaction with the metal is tighter in (**c**) whilst the H-bond network with the couple of Ser and Asn residues is tighter in (**d**). (Color figure available online only.)

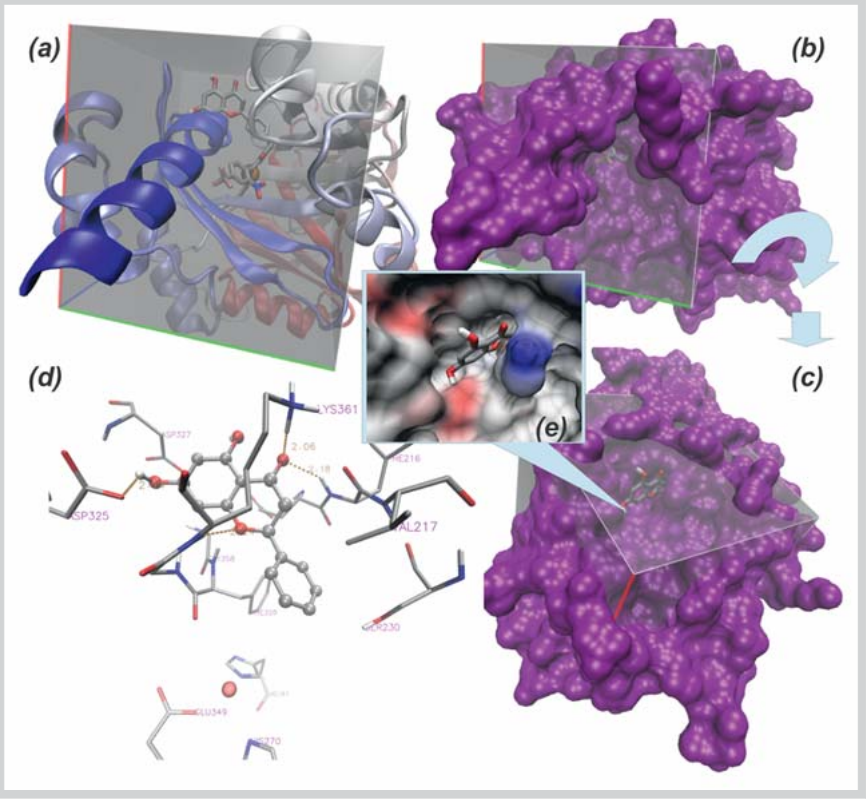

Fig. 7 **a** Cartoon representation of the HPPD in Model II, with the box showing the docking domain where the experimental structure of NTBC and the neutral form of **1** are shown together. The lowest energy structure found for the neutral form of **1** is similar to that found for its anion and it does not overlap with NTBC, which is coordinated to the Fe (II). **b** Molecular surface of the HPPD, showing one entrance to the active site, where part of the CF_3 group of the crystal structure of NTBC appears. The view is rotated in **c**, showing the other entrance to the coordination site where part of the docked structure of **1** appears. **d** Detailed view of the H-bond network and hydrophobic contacts interacting with **1**. **e** Electrostatic potential map at the entrance to the site where the lowest energy docked structure of **1** was found; color ranges according to the electrostatic potential from red (− 5.a. u. [atomic units]) to blue (+ 5 a. u.). (Color figure available online only.)

Finally, the reduced models of the coordination sphere of the Fe (II) were computed with QM calculations (details in Supporting Information) in order to discriminate between the relative strength of the metal coordination, which could just be treated in an *ad hoc* way by means of the docking parameters and the overall effect of all contacts with the protein. The results summarized in **Table 4 S**, Supporting Information, reveal that the neutral form of **1** has a positive enthalpy of complex formation. This means that it is unable to displace two water molecules from the coordination sphere. Therefore, despite the limitations of the docking approach, it is indeed unlikely to mimic the pose of the competitive inhibitors cocrystallized in the experimental struc-

Compound	Free energy of binding/(kcal/mol)	
	Lowest energy structure in the Fe(II) coordination site	Lowest energy structure in the binding domain
Model I		
NTBC	− 7.75	
Mesotrione	− 8.78	
DAS869	− 10.1	
1 (Anionic species)	− 7.09	
1 (Neutral species)	− 6.76	
Model II		
NTBC	− 9.98	− 9.98
Mesotrione	− 11.49	− 11.49
1 (Anionic species)	− 8.55	− 9.80
1 (Neutral species)	− 8.17*	− 9.59

* Not coordinated to Fe(II)

Table 3 Brief summary of docking results.

tures. However, its anionic form showed a similar chelating ability to that of mesotrione, and its complex formation free energy was even slightly more favored by about 10 kcal/mol. This would indicate that the preference of $\mathbf{1}^-$ for another site is not directly related with its chelating ability but with other structural factors, which will be discussed below.

Discussion

The results obtained from screening the anti-HPPD activity of 91 plants from the central region of Argentina showed *F. oolepis, O. charua*, and *S. cuspidata* with the highest effectiveness, with the first of these being the most potent (**Table 1**).

Bioguided fractionation of *F. oolepis* led to the isolation of the flavanone pinocembrin (**1**) (**Fig. 1**). Its inhibitory value (IC_{50} = 18.7 µg/mL; **Table 1**) showed this compound to be almost four times more potent than the crude ethanol extract. The presence of synergism between extract components was thus discarded, pointing to **1** as the only compound responsible for the inhibitory action of the plant. As far as we know, this is the first time that the anti-HPPD effect of **1** has been reported [14, 22–25].

It is worth noting that the average inhibitory concentration of compound **1** (**Table 1**) was of the same order of magnitude as those of isoleptospermone and leptospermone, isolated from *Leptospermum scoparium* J.R. Forst. & G. Forst. and *Callistemon citrinus* (Curtis) Skeels (Myrtaceae) [6, 26], resulting from 50 % inhibition of *Arabidopsis thaliana* (L.) Heynh. (Brassicaceae) HPPD (IC_{50} s of 14.3 and 11.8 µM, respectively) [7]. The differences may be attributed to the different HPPD source.

To gain more insight into the behavior of compound **1** in its interaction with HPPD, its mechanism and mode of inhibition were determined. Compound **1** behaves as a reversible inhibitor. Kinetic analysis showed that **1** binds to HPPD as a noncompetitive inhibitor, and thus the inhibitor can bind with a free enzyme or with an enzyme-substrate complex and the inhibition cannot be overcome by increasing substrate concentration.

Interestingly, deeper insights about the different mechanism of inhibition clearly arose from the molecular modeling study. Both the anionic (**Fig. 6a**) and neutral (**Fig. 7**) form of **1**, when analyzed in the whole binding domain of HPPD, showed greater affinity for the pocket at the entrance of the metal coordination site than for the Fe(II) site itself, where DAS869, mesotrione, and NTBC tightly bind to the metal, as observed in both our docking results and in the experimental crystal structures. This site did not overlap with the site of these inhibitors (see the structures of NTBC and **1** superimposed in **Fig. 7a**), and thus presumably would not overlap with the primary binding of HPP. These docking results are in agreement with the proposal of a noncompetitive inhibition found by kinetics studies. Particularly, in the case of the neutral form of **1** (prevalent at physiological pH), there was no low energy structure mimicking the mode of interaction of the tight-binding inhibitors with the iron.

Following previous explanations, the presence of two carbonyl bonds lying in a plane due to their conjugation in some triketones is a necessary requirement for potent HPPD inhibition [20, 27]. These observations involved mesotrione used as a reference. Compound **1**, which has a similar framework to mesotrione because of its structural rigidity, showed lower activity. The diminished activity could be attributed to the fact the 4-carbonyl group is part of a γ-pyrone six member ring. The fusion of the A and C rings warrants the planarity of the *β*-dioxo system, but it also prevents the flexibility for accommodating the other substituents. This results in a large coordinated plane *π* system (which fits well in the noncompetitive site as shown in **Fig. 7**), in contrast to the crystallographic poses of both NTBC and DAS869 in the Fe(II) coordination sphere, where the *π* conjugation is twisted into two separated planes. On the other hand, the characteristic flavanone B-ring does not seem to be responsible for the different binding mode since it fits well either in the metal coordination site (by *π*-*π* stacking with Phe364) or in the hydrophobic part of the pocket, which shapes the noncompetitive site. However, despite the lower activity of **1** compared to mesotrione, the flavanone could be considered a potent HPPD inhibitor, according to its K_I value (13.7 µM) and in agreement with the considerations of Ling et al. [28].

All the structural data discussed above may help in rationally improving the potency in derivatives of **1** and could be summarized as follows:

1. The quantum calculations of the complexation energies suggest that the anion of **1** is not a poor chelating agent of the Fe(II) coordination site compared to the known potent inhibitors since its results were even better than mesotrione. Thus, its preference for other binding modes should be ascribed to its shape and the role of other substituents (see below). On the other hand, although $\mathbf{1}^-$ seems to act as a ligand of Fe(II), note that mesotrione as well as the crystallographic references DAS869 and NTBC is substantially more acidic than **1**.
2. The free 7-OH group plays a role both in the binding as a bidentate ligand of the iron in the anionic form and in the binding to

the site, where it does not interact with the coordination center. However, in the first case, interaction with the neutral Ser/Asn residues is rather weak, with long distances and unfavored angles, whilst in the second case, it compliments very well with the electrostatic potential of the noncompetitive site and forms a strong H-bond with a charged Asp residue (**Fig. 7**). Another related issue is that none of the inhibitors in the set used to validate the procedures has a free OH in this position relative to the *β*-dioxo system. Moreover, neither NTBC nor DAS869 experimental complexes show H-bond interactions with the couple of Ser/Asn residues. On the contrary, DAS869 exposes its hydrophobic *t*-butyl group to the polar residues and NTBC to its aliphatic ring. In general, as previously noted [2], there was no H-bond interaction found for this kind of inhibitor. Thus, the 7-OH group could be one factor contributing to differentiate the behavior of **1**.

The results shown give evidence about the inhibitory activity, mode, and mechanism of action of compound **1** and its role as a starting structural backbone for the development of semisynthetic or synthetic agents with improved HPPD inhibitory activity. Rational clues about how to derivatize this backbone also arose from the structural analysis presented.

Materials and Methods

Plant materials

Plants were collected in the hills of Córdoba Province, Argentina, from November to December 2005. Most of them were native species with a small number of adventive and introduced plants (**Table 5 S,** Supporting Information). Aerial parts of *F. oolepis* (chilca), the source of the extract to be submitted to isolation, were also collected in March 2006. Previous to performing this process, the activity of the extract was verified. Voucher specimens have been deposited in the "Marcelino Sayago" Herbarium of the School of Agricultural Science, Catholic University of Córdoba and were authenticated by the botanist Gustavo Ruiz (details available as **Table 5 S,** Supporting Information). Plants were selected according to their availability, accessibility, and the lack of scientific information about their inhibition on HPPD.

Crushed aerial plant material was extracted by 48 h maceration with 96% ethanol. The yields of each extract, obtained after solvent removal and expressed as the percentage of weight of air-dried crushed plant material, are shown in **Table 5 S**, Supporting Information.

Chemicals, equipments, and reagents

HPP, mesotrione (Pestanal®, purity 99.9%, by HPLC), and tautomerase from bovine kidney Grade I was purchased from Sigma-Aldrich Co. L-glutathione and 2,6-dichlorophenolindophenol were obtained from Carl Roth and Merck, respectively. Silica gel used for column chromatographies was purchased from Sigma-Aldrich Co. and all solvents were HPLC grade. Analtech silica gel GF plates (2000 microns) were used for preparative TLC. ^{1}H- and ^{13}C-NMR spectra were recorded in DMSO-d_6 (Sigma-Aldrich Co.) with a Bruker AVANCE II 400 spectrometer (Bruker Corporation) operated at 400 MHz for ^{1}H and at 100 MHz for the ^{13}C nucleus. HPLC was performed on a Shimadzu LC-10 AS (Shimadzu Corp.) equipped with a Phenomenex Prodigy 5 µ ODS (4.6 mm i.d. × 250 mm) reversed-phase column, eluting with water/methanol/trifluoracetic acid (TFA) 65 : 35 : 1 as the mobile phase and with UV detection at 365 nm.

Isolation of the 4-hydroxyphenylpyruvate dioxygenase inhibitory compound

The resulting ethanol extract from *F. oolepis* (9.70 g) was subjected to vacuum liquid chromatography on silica gel (427.3 g, 63–200 µm, 11.0 × 24.0 cm; Macherey & Nagel) using a 10% step gradient of hexane/Et_2O (v/v 100% hexane to 100% Et_2O; 200–750 mL, each), Et_2O/AcOEt (v/v 90–10% Et_2O in AcOEt to 100% AcOEt; 250–300 mL, each), and AcOEt/MeOH (v/v 90–10% AcOEt in MeOH to 100% MeOH; 250 mL, each) to yield 30 fractions which were collected in 11 fractions according to TLC monitoring (Fr_1–Fr_{11}). Among these, Fr_3–Fr_4 (4.01 g), eluted with Et_2O 100 (750 mL) to Et_2O/AcOEt 90 : 10 (300 mL), showed inhibitory activity on HPPD with an IC_{50} of 62 µg/mL. After submitting these fractions to column chromatography on silica gel (35–70 µm, 3.0 × 60 cm; Fluka) eluted with a 10% gradient of hexane/Et_2O/acetone, 25 fractions were obtained and combined in 10 fractions (Fr_1-Fr_{10}) according to TLC analysis. Those fractions obtained with hexane/Et_2O 50 : 50 to 25 : 75 showed 70% or higher inhibitory activity at a fixed dose of 50 µg/mL and therefore were rechromatographed in a column chromatography (36.8 g, 35–70 µm, 3.0 × 60 cm; Fluka) eluted with a 10% step gradient of hexane/Et_2O starting on 100% hexane to 100% Et_2O to yield 35 fractions combined in seven fractions (Fr_1–Fr_7). A solid, identified by NMR as 5,7-dihydroxyflavanone or pinocembrin (**1**) [14] (**Fig. 1**; copies of the original spectra are obtainable from the corresponding author), was obtained by spontaneous crystallization (99% purity by HPLC; yield: 1.14 g/100 g of crushed plant material and 4.95 g/100 g of extract) from active Fr_5 eluted with hexane/Et_2O 50 : 50.

The remaining active impure mixture, containing only pinocembrin and another substance, was further purified by preparative TLC to finally obtain orange-yellow needles. This solid, identified by NMR as 2′,4′-dihydroxychalcone [29] (99% purity by HPLC; yield: 1.24/100 g of crushed plant material; copies of the original spectra are obtainable from the corresponding author), showed no effectiveness against HPPD (IC_{50} = 456.7 µM).

4-Hydroxyphenylpyruvate dioxygenase preparation

HPPD was extracted from porcine liver acetone powder. This source was chosen due to the high similarity (more than 80%) between this enzyme and that of human origin [30]. For the preparation of the powder, the method described by Taniguchi and Armstrong [31] was followed. Briefly, 200 g of fresh liver were homogenized with 200 mL of cold phosphate buffer (50 mM, pH 7.4). Then, the slurry was stirred for 5 min at 4 °C with 3 L of cold acetone. The resulting homogenate was filtered and the residue was washed with cold acetone and then peroxide-free ether. After drying at room temperature, the solid was sieved. The resulting powder (60 g) was extracted for 2 h with the phosphate buffer at 4 °C as described in Roche et al. [32]. After centrifugation at 16300 g for 30 min at 4 °C, a glutathione solution (0.1 mg/mL) was added to the supernatant. This was fractioned and stored at − 20 °C as a source of HPPD [32]. The protein concentration was determined as 28.77 mg/mL using the Bradford method (BioRad Laborarories) with bovine serum albumine as the calibrating protein. This preparation presented an HPPD-specific activity of 183.5 units/mL, defining 1 unit as the increase in absorbance of 0.001/min.

p-Hydroxyphenylpyruvate dioxygenase inhibitory assay

The inhibitory activity of HPPD was determined spectrophotometrically with the enol-borate tautomerase method following the technique reported by Schulz et al. [33] with some modifications. Briefly, 150 µL of HPP 1.8 mM, 300 µL of a mixture of 100 µL of glutathione 166 mM and 1000 µL of 2,6-dichlorophenolindophenol 3.3 mM (freshly prepared), and 10 µL of tautomerase (10 U/mL) were added to 8500 µL of borate buffer (0.42 M adjusted to pH 6.2 with 0.25 M Na_2HPO_4). The tautomerization was allowed to equilibrate at room temperature, measuring the increase in absorbance at 308 nm due to the enol-borate complex formation [34]. Then, 10 µL of a solution of the extracts or compounds, previously dissolved in ethanol, or of each fraction obtained in the isolation processes dissolved in DMSO, was added to 950 µL of the reagent mixture. Finally, 40 µL of enzyme preparation was added. Extracts were first tested at 250 µg/mL and those showing 85% inhibition or higher in three different repetitions were further evaluated for the concentration necessary for 50% inhibition (IC_{50}). Controls containing only ethanol or DMSO were simultaneously run. Mesotrione dissolved in DMSO (final concentration = 250 µg/mL) was used as a positive control.

The reaction was run at 25 °C following the decrease in absorbance monitored at 308 nm from time 0 and thereafter at 10 min intervals. The reaction extent was determined by the difference in absorbance at 10 and at 40 min and the percentage of inhibition was calculated according to the following equation (1):

$$\text{Inhibition}(\%) = 100 - \left[\frac{\Delta\text{Abs}_{\text{sample}} \times 100}{\Delta\text{Abs}_{\text{control}}}\right] \quad (1)$$

The mechanism by which **1** inhibits the enzyme was further investigated through the graph of the relationship of the enzyme activity with its concentration in the presence of different concentrations of the inhibitor. Under the conditions employed in this study, the enzymatic reaction follows a Henri-Michaelis-Menten equation, and the kinetic of the enzyme was therefore studied using the Lineweaver-Burk double-reciprocal plot of velocity in the function of different substrate concentrations (after tautomerization). The inhibition constant K_I was obtained from the second plot of the vertical intercept ($1/V_{max}^{app}$) of the double-reciprocal lines versus the concentration of compound **1**. K_I is represented by the equation (2):

$$\text{Intercept} = \frac{1}{K_I V_{max}}[I] + \frac{1}{V_{max}} \quad (2)$$

Molecular modeling

Ab initio calculations on the active site and inhibitors, and preparation of the models for docking: HPPD is a non-heme iron (II)-dependent metalloenzyme. It has been suggested [1,35] that the coordination site of the Fe(II) of the free enzyme may be described by a fast equilibrium between the pentacoordinated and hexacoordinated forms (two histidines, the glutamate, and two or three water molecules, respectively). In order to obtain a reliable charge distribution for the docking simulations, QM calculations were performed at the CAM-B3LYP/LACVP [36] level of theory on reduced models of the site including the Fe(II) ion, two (or three) coordinated water molecules, and the coordinated residues capped at their α-carbons. This approach had already been satisfactorily used for describing a more complex (dinuclear) metal coordination site [13]. The RESP charges [37] were obtained from the quantum results, and the solvation parameters for Fe(II) had an effective radius of 1.3 Å for RESP fitting. The rest of the protein was charged as previously [13] using Gasteiger charges (Autodock 4.2 program default) [38] (further details available as Supporting Information). Even though divalent iron is expected to form high spin complexes, no assumptions were made about the actual spin state and all possibilities were calculated. The reduced model of the active site was therefore simulated as a singlet, triplet, quintet, and heptuplet. Since the quintet (S = 2) was found to be the most stable state, this was used for further QM calculations and for setting up the docking protocol (for details see **Table 6 S**, Supporting Information). The structures of the most stable conformers of the inhibitors were obtained by full geometry optimization using the same level of theory as in the calculations of the coordination site model. The nature of minima of the stationary points was established by means of harmonic frequency analysis using the Gaussian 09 package [39].

General docking setup: The binding mode of **1** was analyzed *in silico* by docking it to a mammal structure of the HPPD from *Ratus novergicus* (PDB entry 1SQI) complexed with the DAS869 inhibitor. The binding was compared with the inhibitor NTBC onto the HPDD from *Streptomyces avermitilis* (PDB entry 1T47) as more accurate and complete information is available for this protein. For both structures and by considering both penta- and hexacoordinations (see Supporting Information for further details), different models were built (see below) and all of these were validated by evaluating their performance in the following tests:

1. Blind docking was intended to reproduce the experimental inhibitor/protein structures since *R. novergicus* and *S. avermitilis* proteins were cocrystallized with DAS869 [21] and NTBC [15] (chemical structures in **Fig. 4**), respectively. All the models built were challenged to reproduce the experimental pose of the inhibitor in the crystal.
2. The correlation of the binding energies was estimated by docking against a panel of 13 experimental IC_{50} s for the compounds shown in **Fig. 4** [15–21]. The set includes 10 di- and triketone-related compounds with known activity, mesotrione, which was measured in this work as a known inhibitor, DAS869, and NTBC.

A summary of the models built and subjected to the above experimental correlations is as follows:

- Model I: *R. novergicus* HPPD with one water molecule coordinated.
- Model II: *S. avermitilis* HPPD with all water molecules removed.
- Model III: as Model I but with the water molecule removed.
- Model IV: as Model II but with one water molecule coordinated.
- Model V: as Model I but with flexible His336, His364, and water molecule.
- Model VI: as Model II but with flexible His336 and His364.

The results obtained only from Models I and II were discussed in the main text since they yielded the best correlations with the experiments for each structure after applying the validation procedures described above (for further details see **Tables 2 S** and **3 S**, Supporting Information). The data regarding the rest of the models, which showed similar trends but lower correlation indexes (with R^2 ranging from 0.706 to 0.867), are summarized in **Fig. 4 S, 5 S, 6 S** and **7 S**, Supporting Information.

Since the evaluated compounds A–M (**Fig. 4**) could present different tautomer and protonation states, the ligand structures used for the docking procedures in each case corresponded to that which is more likely to exist at physiological pH. With this

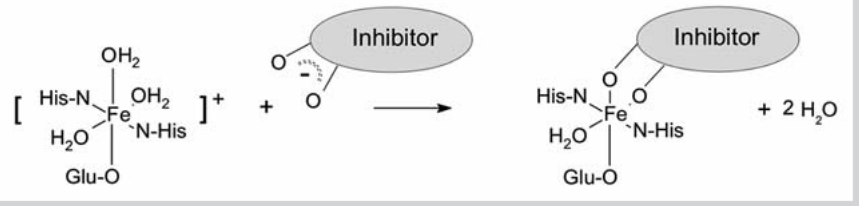

Fig. 8 Schematic representation of the reaction of FE(II) chelation by inhibitors.

in mind, computational simulations of the pKa's of the tautomeric forms of compounds A–M were performed using ACD/Labs software [40,41] (details available in **Table 7 S**, Supporting Information). The pKa values (both calculated and experimentally reported, when available) found for all the assayed compounds were below 7, and therefore the anionic form was the one used for calculation, as drawn in **Fig. 4**. However, for our subject compound **1**, as its pKa was 7.56, close to the physiological pH, both the neutral and phenolate forms were simulated and analyzed in detail.

The Autodock 4.2 package [38,42] was used for the docking simulations, and analysis and visualization of the results were made using both MGLTools 1.5.4 [38] and VMD 1.8.9 [43] (further details available as Supporting Information).

Evaluating the chelating ability of 1 and mesotrione by quantum calculations

Finally, reduced models of the active site of the HPPD were used for calculating the chelating ability of mesotrione and the neutral and phenolic forms of **1**. The estimated ΔGs for the reaction on **Fig. 8** were obtained from the total energies at the CAM-B3LYP/LACVP+ level of theory without zero point corrections (details available as Supporting Information) both *in vacuum* and using an implicit solvation model (IEFPCM) with a dielectric constant of 12.8 [44–46].

Statistical analysis

The results are expressed as the mean ± SE obtained by Infostat Software, 2008. The IC_{50} was calculated by log-Probit analysis responding to five concentrations of each extract, active fractions, or compound by duplicate in two different experiments at the 95% confidence level with upper and lower confidence limits.

Supporting information

Complete information about tested plants and their activity together with information about the molecular modeling are available as Supporting Information.

Acknowledgements

This work was supported by the Catholic University of Córdoba, FONCYT (BID 1728 33593, PICTO CRUP 6–31396 and PICT 0141), MINCyT Córdoba (GRF 2008) and CONICET (PIP 11220100 100236). M.E.C., L.T., M.B.J., and G.N.D.N. acknowledge the receipt of a scholarship from CONICET. We thank Joss Heywood for revising the English language. We also thank Diego Lescano of Biofarma S.A. for supplying pig livers. M.C. Carpinella, D.M.A. Vera, and S.M. Palacios are staff members of the National Research Council of Argentina (CONICET).

Conflict of Interest

The authors declare no conflict of interest.

References

1 *Moran GR.* 4-Hydroxyphenylpyruvate dioxygenase. Arch Biochem Biophys 2005; 433: 117–128
2 *Moran GR.* 4-Hydroxyphenylpyruvate dioxygenase and hydroxymandelate synthase: exemplars of the α-keto acid dependent oxygenases. Arch Biochem Biophys 2014; 544: 58–68
3 *Imtiaz F, Rashed MS, Al-Mubarak B, Allam R, El-Karaksy H, Al-Hassnan Z, Al-Owain M, Al-Zaidan H, Rahbeeni Z, Qari A, Meyer BF, Al-Sayed M.* Identification of mutations causing hereditary tyrosinemia type I in patients of Middle Eastern origin. Mol Genet Metab 2011; 104: 688–690
4 *Neve S, Aarenstrup L, Tornehave D, Rahbek-Nielsen H, Corydon TJ, Roepstorff P, Kristiansen K.* Tissue distribution, intracellular localization and proteolytic processing of rat 4-hydroxyphenylpyruvate dioxygenase. Cell Biol Int 2003; 27: 611–624
5 *Raspail C, Graindorge M, Moreau Y, Crouzy S, Lefèbvre B, Robin AY, Dumas R, Matringe M.* 4-hydroxyphenylpyruvate dioxygenase catalysis: identification of catalytic residues and production of a hydroxylated intermediate shared with a structurally unrelated enzyme. J Biol Chem 2011; 286: 26061–26070
6 *Dayan FE, Duke SO, Sauldubois A, Singh N, McCurdy C, Cantrell C. p*-Hydroxyphenylpyruvate dioxygenase is a herbicidal target site for *β*-triketones from *Leptospermum scoparium*. Phytochemistry 2007; 68: 2004–2014
7 *Dayan FE, Singh N, McCurdy CR, Godfrey CA, Larsen L, Weavers RT, Van Klink JW, Perry NB. β*-Triketone inhibitors of plant *p*-hydroxyphenylpyruvate dioxygenase: modeling and comparative molecular field analysis of their interactions. J Agric Food Chem 2009; 57: 5194–5200
8 *Hüter O.* Use of natural products in the crop protection industry. Phytochem Rev 2011; 10: 185–194
9 *Meazza G, Scheffler BE, Tellez MR, Rimando AM, Romagni JG, Duke SO, Nanayakkara D, Khan IA, Abourashed EA, Dayan FE.* The inhibitory activity of natural products on plant *p*-hydroxyphenylpyruvate dioxygenase. Phytochemistry 2002; 60: 281–288
10 *Balunas MJ, Kinghorn AD.* Drug discovery from medicinal plants. Life Sci 2005; 78: 431–441
11 *Carpinella MC, Andrione DG, Ruiz G, Palacios SM.* Screening for acetylcholinesterase inhibitory activity in plant extracts from Argentina. Phytother Res 2010; 24: 259–263
12 *Chiari ME, Joray MB, Ruiz G, Palacios SM, Carpinella MC.* Tyrosinase inhibitory activity of native plants from central Argentina: Isolation of an active principle from *Lithrea molleoides*. Food Chem 2010; 120: 10–14
13 *Chiari ME, Vera DMA, Palacios SM, Carpinella MC.* Tyrosinase inhibitory activity of a 6-isoprenoid-substituted flavanone isolated from *Dalea elegans*. Bioorg Med Chem 2011; 19: 3474–3482
14 *Diaz Napal GN, Carpinella MC, Palacios SM.* Antifeedant activity of ethanolic extract from *Flourensia oolepis* and isolation of pinocembrin as its active principle compound. Bioresour Technol 2009; 100: 3669–3673
15 *Brownlee JM, Johnson-Winters K, Harrison DHT, Moran GR.* Structure of the ferrous form of (4-hydroxyphenyl)pyruvate dioxygenase from *Streptomyces avermitilis* in complex with the therapeutic herbicide, NTBC. Biochemistry (Mosc) 2004; 43: 6370–6377
16 *Ellis MK, Whitfield AC, Gowans LA, Auton TR, Provan WM, Lock EA, Lee DL, Smith LL.* Characterization of the interaction of 2-[2-nitro-4-(trifluoromethyl)benzoyl]-4,4,6,6-tetramethylcyclohexane-1,3,5-trione with rat hepatic 4-hydroxyphenylpyruvate dioxygenase. Chem Res Toxicol 1996; 9: 24–27

17 *Lee DL, Knudsen CG, Michaely WJ, Chin HL, Nguyen NH, Carter CG, Cromartie TH, Lake BH, Shribbs JM, Fraser T.* The structure-activity relationships of the triketone class of HPPD herbicides. Pestic Sci 1998; 54: 377–384

18 *Lin SW, Lin YL, Lin TC, Yang DY.* Discovery of a potent, non-triketone type inhibitor of 4-hydroxyphenylpyruvate dioxygenase. Bioorg Med Chem Lett 2000; 10: 1297–1298

19 *Lin YL, Wu CS, Lin SW, Yang DY.* SAR studies of 2-o-substituted-benzoyl- and 2-alkanoyl-cyclohexane-1,3-diones as inhibitors of 4-hydroxyphenylpyruvate dioxygenase. Bioorg Med Chem Lett 2000; 10: 843–845

20 *Wu CS, Huang JL, Sun YS, Yang DY.* Mode of action of 4-hydroxyphenylpyruvate dioxygenase inhibition by triketone-type inhibitors. J Med Chem 2002; 45: 2222–2228

21 *Yang C, Pflugrath JW, Camper DL, Foster ML, Pernich DJ, Walsh TA.* Structural basis for herbicidal inhibitor selectivity revealed by comparison of crystal structures of plant and mammalian 4-hydroxyphenylpyruvate dioxygenases. Biochemistry (Mosc) 2004; 43: 10414–10423

22 *Rasul A, Millimouno FM, Ali Eltayb W, Ali M, Li J, Li X.* Pinocembrin: a novel natural compound with versatile pharmacological and biological activities. Biomed Res Int 2013; 2013: 379850

23 *Liu R, Li JZ, Song JK, Sun JL, Li YJ, Zhou SB, Zhang TT, Du GH.* Pinocembrin protects human brain microvascular endothelial cells against fibrillar amyloid-β(1 – 40)injury by suppressing the MAPK/NF-κB inflammatory pathways. Biomed Res Int 2014; 2014: 470393

24 *Yang N, Qin S, Wang M, Chen B, Yuan N, Fang Y, Yao S, Jiao P, Yu Y, Zhang Y, Wang J.* Pinocembrin, a major flavonoid in propolis, improves the biological functions of EPCs derived from rat bone marrow through the PI3 K-eNOS-NO signaling pathway. Cytotechnology 2013; 65: 541–551

25 *Meng F, Wang Y, Liu R, Gao M, Du G.* Pinocembrin alleviates memory impairment in transient global cerebral ischemic rats. Exp Ther Med 2014; 8: 1285–1290

26 *Barton AF, Dell B, Knight AR.* Herbicidal activity of cineole derivatives. J Agric Food Chem 2010; 58: 10147–10155

27 *Lee DL, Prisbylla MP, Cromartie TH, Dagarin DP, Howard SW, Mc Lean Povan W, Ellis MK, Fraser T, Mutter LC.* The discovery and structural requirements of inhibitors of *p*-hydroxyphenylpyruvate dioxygenase. Weed Sci 1997; 45: 601–609

28 *Ling TS, Shiu S, Yang DY.* Design and synthesis of 3-fluoro-2-oxo-3-phenylpropionic acid derivatives as potent inhibitors of 4-hydroxyphenylpyruvate dioxygenase from pig liver. Bioorg Med Chem 1999; 7: 1459–1465

29 *Barrero AF, Herrador MM, Arteaga P, Rodríguez-García I, García-Moreno M.* Resorcinol derivatives and flavonoids of *Ononis natrix* subspecies *ramosissima.* J Nat Prod 1997; 60: 65–68

30 *Rüetschi U, Dellsén A, Sahlin P, Stenman G, Rymo L, Lindstedt S.* Human 4-hydroxyphenylpyruvate dioxygenase. Eur J Biochem 1993; 213: 1081–1089

31 *Taniguchi K, Armstrong MD.* The enzymatic formation of o-hydroxyphenylacetic acid. J Biol Chem 1963; 238: 4091–4097

32 *Roche PA, Moorehead TJ, Hamilton GA.* Purification and properties of hog liver 4-hydroxyphenylpyruvate dioxygenase. Arch Biochem Biophys 1982; 216: 62–73

33 *Schulz A, Ort O, Beyer P, Kleinig H.* SC-0051, a 2-benzoyl-cyclohexane-1, 3-dione bleaching herbicide, is a potent inhibitor of the enzyme *p*-hydroxyphenylpyruvate dioxygenase. FEBS Lett 1993; 318: 162–166

34 *Knox WE, Pitt BM.* Enzymic catalysis of the keto-enol tautomerization of phenylpyruvic acids. J Biol Chem 1957; 225: 675–688

35 *Neidig ML, Kavana M, Moran GR, Solomon EI.* CD and MCD Studies of the non-heme ferrous active site in (4-hydroxyphenyl)pyruvate dioxygenase: correlation between oxygen activation in the extradiol and α-KG-dependent dioxygenases. J Am Chem Soc 2004; 126: 4486–4487

36 *Yanai T, Tew DP, Handy NC.* A new hybrid exchange–correlation functional using the Coulomb-attenuating method (CAM-B3LYP). Chem Phys Lett 2004; 393: 51–57

37 *Bayly CI, Cieplak P, Cornell W, Kollman PA.* A well-behaved electrostatic potential based method using charge restraints for deriving atomic charges: the RESP model. J Phys Chem 1993; 97: 10269–10280

38 *Morris GM, Goodsell DS, Halliday RS, Huey R, Hart WE, Belew RK, Olson AJ.* Automated docking using a Lamarckian genetic algorithm and an empirical binding free energy function. J Comput Chem 1998; 19: 1639–1662

39 *Frisch MJ, Trucks GW, Schlegel HB, Scuseria GE, Robb MA, Cheeseman JR, Scalmani G, Barone V, Mennucci B, Petersson GA, Nakatsuji H, Caricato M, Li X, Hratchian HP, Izmaylov AF, Bloino J, Zheng G, Sonnenberg JL, Hada M, Ehara M, Toyota K, Fukuda R, Hasegawa J, Ishida M, Nakajima T, Honda Y, Kitao O, Nakai H, Vreven T, Montgomery JA jr., Peralta JE, Ogliaro F, Bearpark M, Heyd JJ, Brothers E, Kudin KN, Staroverov VN, Kobayashi R, Normand J, Raghavachari K, Rendell A, Burant JC, Iyengar SS, Tomasi J, Cossi M, Rega N, Millam JM, Klene M, Knox JE, Cross JB, Bakken V, Adamo C, Jaramillo J, Gomperts R, Stratmann RE, Yazyev O, Austin AJ, Cammi R, Pomelli C, Ochterski JW, Martin RL, Morokuma K, Zakrzewski VG, Voth GA, Salvador P, Dannenberg JJ, Dapprich S, Daniels AD, Farkas O, Foresman JB, Ortiz JV, Cioslowski J, Fox DJ.* Gaussian 09, Revision A.01. Wallingford CT: Gaussian, Inc.; 2009

40 *ACD labs.* Predict accurate acid/base dissociation constants from structure – the industry standard. Available at http://www.acdlabs.com/products/percepta/predictors/pka/. Accessed 17 August 2015.

41 *Liao C, Nicklaus MC.* Comparison of nine programs predicting pKa values of pharmaceutical substances. J Chem Inf Model 2009; 49: 2801–2812

42 *Morris GM, Huey R, Lindstrom W, Sanner MF, Belew RK, Goodsell DS, Olson AJ.* AutoDock4 and AutoDockTools4: Automated docking with selective receptor flexibility. J Comput Chem 2009; 16: 2785–2791

43 *Humphrey W, Dalke A, Schulten K.* VMD: visual molecular dynamics. J Mol Graph 1996; 14: 33–38

44 *Cancès E, Mennucci B.* Comment on "Reaction field treatment of charge penetration" [J Chem Phys 112, 5558 (2000)]. J Chem Phys 2001; 114: 4744–4745

45 *Chipman DM.* Reaction field treatment of charge penetration. J Chem Phys 2000; 112: 5558–5565

46 *Tomasi J, Mennucci B, Cances E.* The IEF version of the PCM solvation method: an overview of a new method addressed to study molecular solutes at the QM ab initio level. J Mol Struc: THEOCHEM 1999; 464: 211–226